Available online at www.sciencedirect.com
ScienceDirect
Journal of Volcanology and Geothermal Research 158 (2006) 51–69
Journal of volcanology and geothermal research
www.elsevier.com/locate/jvolgeores

Pleistocene mafic volcanoes in the Puna–Cordillera Oriental boundary, NW-Argentina

S.R. Guzmán [a,*], I.A. Petrinovic [a], J.A. Brod [b]

[a] CONICET-IBIGEO, Museo de Ciencias Naturales, UNSa. Mendoza 2-4400, Salta, Argentina
[b] Instituto de Geociências, Universidade de Brasília. Campus Asa Norte, 70.910-900 Brasília, Brasil

Received 31 December 2004; accepted 10 April 2006
Available online 15 June 2006

Abstract

Los Gemelos and El Saladillo are both monogenetic, strombolian, basaltic–shoshonitic volcanoes that constitute the easternmost recognized examples of mafic Plio-Quaternary volcanism in the southern Central Andes. Two regional faults delimit the borders of the Calchaquí valley, as thrusts with opposite vergence: the eastern Calchaquí fault and the western Toro Muerto fault. While Los Gemelos are set in the hanging wall of Calchaquí back-thrust fault, El Saladillo are set in the footwall of Toro Muerto fault. As Los Gemelos volcanoes have well preserved morphological features, we highlight some relationship between them and their tectonic setting. Kinematic data and one new measurement, that indicate right strike-slip movement in the vicinity of Los Gemelos during the Pleistocene–Holocene. The emplacement of these volcanoes should be related to a transpression zone parallel to the valley, where the alignment of the cones is outlining the trend of conjugated faults.

The magmas were derived from a small degree of partial melting of an enriched, garnet-bearing mantle source. The analysed rocks have primitive signature (high Ni, Cr, Co and MgO concentrations; presence of chromite and forsteritic olivine) and evidence for crustal contamination with felsic rocks (quartz±plagioclase±K-feldspar xenocrysts with coronas, reaction rims and/or embayments; high $^{87}Sr/^{86}Sr$ ratios, negative εNd values). The high Cr and Ni content, high Mg# and low crystal content suggest that no major fractional crystallization occurred, therefore precluding long residence periods. Rapid magma ascent across 60 km of continental crust was guided by magmatic overpressure favoured by important tectonic stresses also avoiding significant residence time at upper crust depth. Thus, we invoke a process of assimilation during turbulent ascent (ATA) to explain the contamination at crustal levels.

Los Gemelos volcanoes were formed around 35,000 yr. as inferred from the age of lacustrine sediments overlying the lava flows. These ages agree well with the age of paleolakes of tectonic origin in NW Argentina, suggesting a common tectonic cause for both effects.

Keywords: Central Andes; El Saladillo; Los Gemelos; shoshonite; ATA

1. Introduction

The Neogene magmatism in the Southern Central Andes is a response to the interaction between the Nazca and South American plates and is distributed between 16°S and 27°S defining the Central Volcanic Zone

* Corresponding author. Tel.: +54 387 4318086; fax: +54 387 4255483.
E-mail address: sguzman@unsa.edu.ar (S.R. Guzmán).

0377-0273/$ - see front matter © 2006 Elsevier B.V. All rights reserved.
doi:10.1016/j.jvolgeores.2006.04.014

(Barazangi and Isacks, 1976), where the subduction angle is about 30°, and where the continental crust is 35–70 km thick (Yuan et al., 2002).

Plio-Quaternary monogenetic centres, mafic in composition (basaltic andesites) are mainly distributed in the Southern Puna and along the Calama–Olacapato–Toro lineament in a back-arc position (Deruelle, 1982; Viramonte et al., 1984; Kay et al., 1994), and are located 220 km above the subducted slab. Knox et al. (1989) recognized three compositionally distinct magma types among the Puna basaltic andesites: a shoshonitic group, the Galan-type group and a high K calc-alkaline group.

Los Gemelos (24° 45′ S–66° 10′W) and El Saladillo (24° 33′ 23″S–66° 12′ 10″W) belong to the shoshonitic group. According to Kay et al. (1994) this specific group lay above a non-delaminated thickened crust. Moreover, this magmatism is spatially and temporally associated with regional structures (Marrett, 1990; Marrett et al., 1994; Riller et al., 1999; Riller and Oncken, 2003), and might be related to a change in the

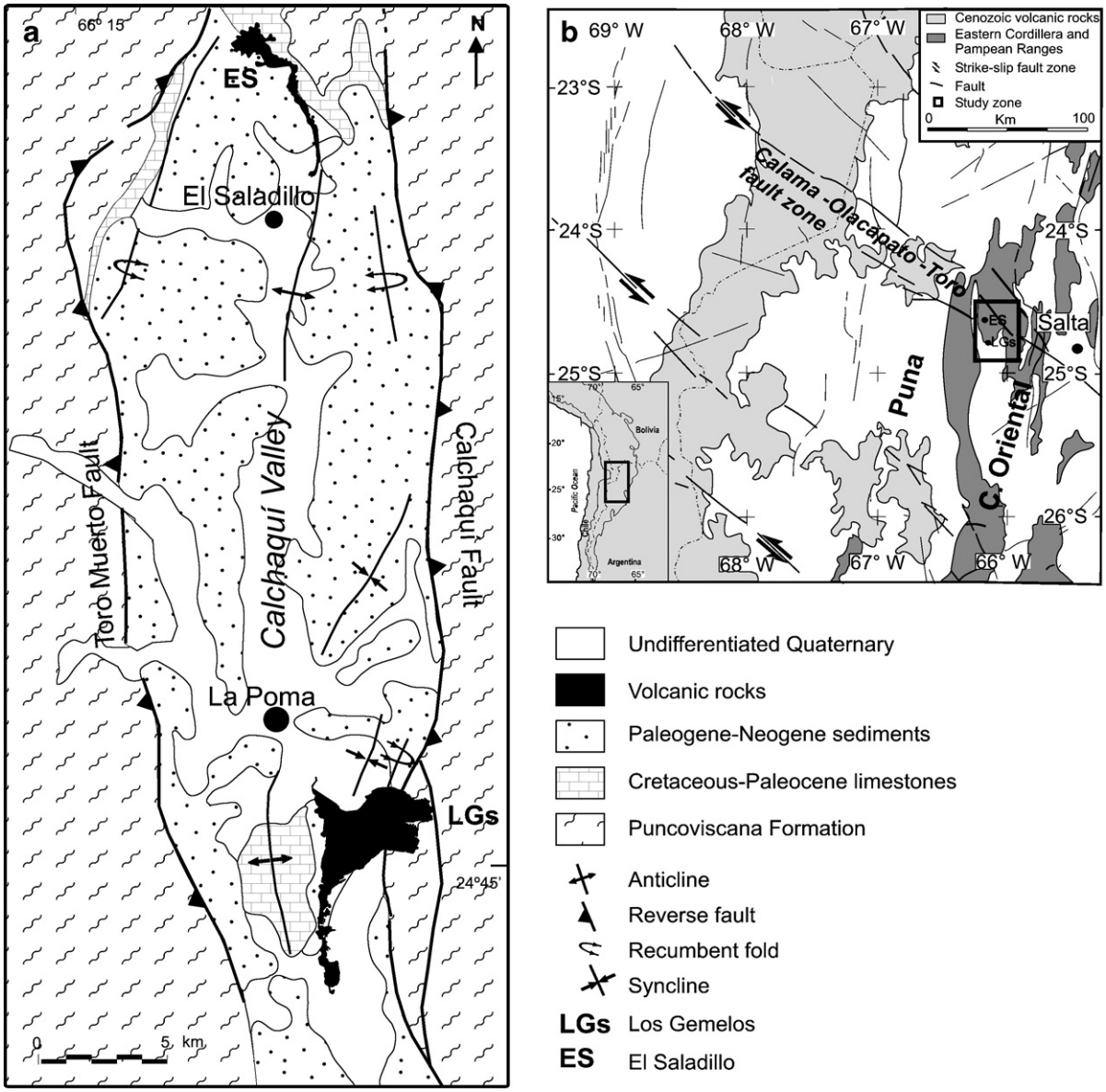

Fig. 1. a) Geological map of north Calchaquí valley (modified from Riller et al., 1999), b) Calama–Olacapato–Toro volcanic belt map modified from Petrinovic et al., 2005. Rectangle shows the area of (a) while the square in South America map indicates the relative position in the Calama–Olacapato–Toro volcanic belt.

deformation regime during the Plio-Pleistocene (e.g. Marrett, 1990).

Although these volcanic edifices represent the easternmost mafic Plio-Quaternary magmatism (near the arc-foreland boundary) outlining regional N–S trending structures, they were not studied in detail so far. In this work, we present cartography of each volcanic edifice and their products, and estimate Los Gemelos age. Additionally, we present new geochemical data including major, trace and REE elements, isotopic ratios and mineral chemistry analyses. We also make some comparisons with other monogenetic centres. Finally, alternative petrogenetic considerations are made in order to explain the origin and ascent of the primary magmas based on petrography, mineral chemistry, isotopic ratios and whole-rock chemistry.

2. Geological background

The Los Gemelos (LGs) and El Saladillo (ES) volcanoes are located in the northern Calchaquí valley (Fig. 1a and b), a structural depression — separating the Puna and Cordillera Oriental — limited by two regional thrusts opposite in vergence (Calchaquí fault and Toro Muerto fault: Fig. 1a).

Both Calchaquí and Toro Muerto faults uplifted Precambrian–Early Cambrian blocks made up of the Puncoviscana Formation above sandstones, pelites and limestones of the Cretaceous–Eocene Salta Group and/or the Payogastilla Group of the Paleogene–Neogene foreland basin. Quaternary sediments include lacustrine and alluvial–fluvial deposits. While Los Gemelos volcanoes are set in the Puncoviscana Formation (Fig. 2a) the El Saladillo volcano is set in Cretaceous–Paleocene sediments, in the downthrown block of Toro Muerto fault (Fig. 2b). The age and kinematics of faults that limit the Calchaquí valley are currently a matter of debate. Marrett (1990) interprets a first stage of overthrusts that generated post-Oligocene NW–SE subhorizontal compression followed by a stage of recent deformation with NE–SW subhorizontal shortening and/or NW extension with subhorizontal right lateral slip, giving way to pull-apart structures. Alternatively, Mon and Salfity (1995) and later Riller and Oncken (2003) argue for a left lateral transpression, active at least since the Miocene at the northern Calchaquí valley. In the uplifted block of the Calchaquí fault, oblique right handed fault planes with strike-slip components were determined at about 10° from the trace of the main thrust (Fig. 2a), supporting the structural model of Marrett et al. (1994), where the thrusts that limit the valley have a right strike-slip component. At present, the Calchaquí fault remains active, as evidenced by the increment in the slope of Pleistocene–Holocene alluvial cones, and, more directly, by the earthquake of 24/12/1930 which destroyed

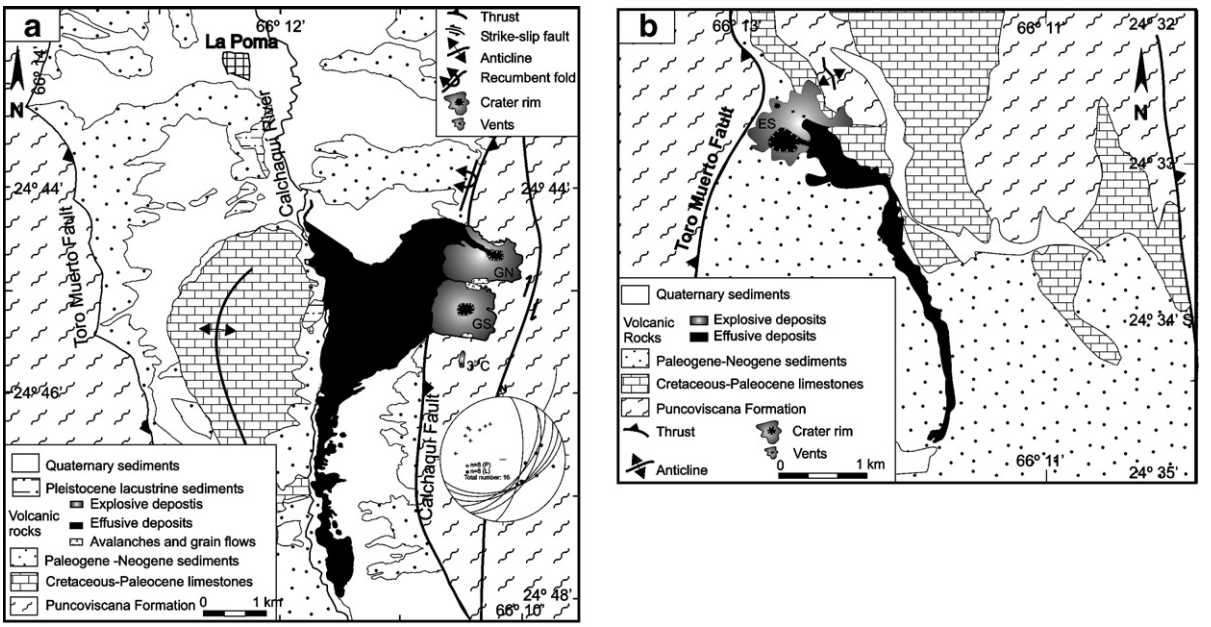

Fig. 2. a) Simplified geological map of La Poma surroundings. Symbols in stereographic lower-hemisphere equal-area projections are: crosses: poles to oblique fault planes, filled circles are poles to striae measurements. b) Simplified geological map of El Saladillo volcano region.

La Poma village and had a magnitude of 6 (Instituto Nacional de Prevención Sísmica de Argentina).

3. Field descriptions

Los Gemelos volcanoes overlie Puncoviscana Formation (Fig. 2a) while their lavas are overlain by lacustrine sediments and alluvial fans.

The Los Gemelos of La Poma volcanoes are two scoria cones (Gemelo Norte "GN" and Gemelo Sur "GS", Fig. 2a) and a third eruptive conduit (3rd C) approximately aligned at N20°. The bases of the cones (GN and GS) and their craters are slightly elongated in an E–W direction (Fig. 2a). A fissure opening (3rd C) is recognized 500 m SSW of the GS volcano (Fig. 2a).

The volcanic products and vertical facies relations in the cones are typical of strombolian eruptions: poorly stratified air-fall deposits with scarce selection and repose angles of about 30°; occurrence of dense lava slabs, breadcrust bombs, pahoehoe to mainly blocky lavas and medium vesiculation of the fragments. Syn-depositional features such as fragments welding and agglutination due to compaction and amalgamation are common. During construction of the cones, some small avalanches (dense packing) and grain flow deposits (reverse gradation) were formed in the flanks of the cones due to the fall of pyroclasts on unstable slopes. All these deposits are composed of lapilli to block-sized (2 mm up to 30 cm), black, generally angular fragments and vesiculated scoriae, smaller amounts of bombs (reaching 40 cm) and slabby blocks of dense lavas. The blocks (Fig. 3a) are interpreted to represent plugs of lava that cooled at the conduit surface and were then explosively ejected.

These pyroclastic deposits were followed by lava effusion, with an estimated magma volume of 0.45 km^3

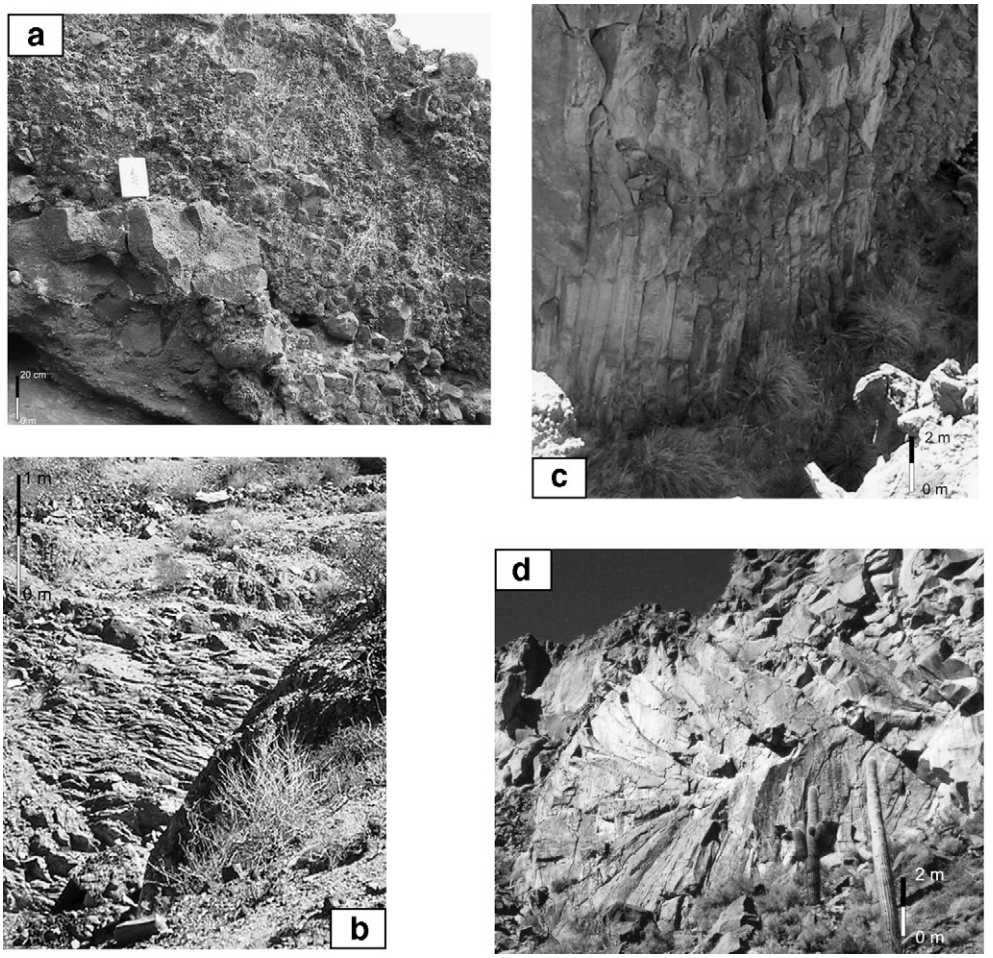

Fig. 3. a) Slabby block of dense lava interbbeded in air-fall deposits, b) ropy pahoehoe lavas, c) columnar jointing in lavas from Los Gemelos volcanoes, and d) radial jointing in lavas from Los Gemelos volcanoes.

(vesiculated) considerably larger than the volume extruded during the explosive phase (0.068 km^3 vesiculated). At least three lava flows emerged from GN volcano — with NW, W and SW exit directions — one of them breaching GN crater. All flowed westwards to reach the Calchaquí river where they joined and silted up the river channel, running it from North to South (Fig. 2a). The GS volcano emitted at least two lava flows separated by fine-grained material of chaotic distribution. They emerged from altitudes lower than the crater, through lateral conduits. Few ropy pahoehoe lavas (Fig. 3b) are preserved at zones of high slope, evolving to blocky lavas towards distal facies where they channelize and show columnar (Fig. 3c) and radial jointing (Fig. 3d). The third eruptive conduit, to the south of GS corresponds to a fissure opening and emitted fall out deposits of reduced dispersion; the first stage of conduit opening is marked by a fine-grained fall out deposit and by the presence of a significant amount (5%) of country rock clasts. This is followed by fall-out material of coarser, lapilli to block-sized scoriae.

El Saladillo are a set of monogenetic cones that lay above deposits from the Salta Group. The most developed of these volcanoes corresponds to a spatter cone with a semicircular crater 200 m in diameter. Some lavas emitted by this centre overflowed the crater rim forming a lava tunnel whose roof collapsed afterwards, leaving a ravine 10 m deep. At the end, a compact central lava body occupied the crater centre. A partially eroded scoria cone is recognized 100 m north-westwards from this cone. It is composed of coarse-grained fall-out materials and slabby blocks of dense lava. The repose angle of these 5-m thick deposits is lower than 10°. In addition, smaller cones (Fig. 2b) of solely explosive activity were formed. The lavas emitted by El Saladillo are massive in proximal facies and blocky in more distal facies.

4. Petrography and mineral chemistry

Chemical analyses of selected minerals were performed by WDS with a Cameca SX-50 electron microprobe operating at 15 kV and 25 nA at the Instituto de Geociências, Universidade de Brasilia. Analyses were calibrated with both natural and synthetic reference materials. The analytical errors are below 2% of the concentration for major elements and below 5% of the concentration for minor elements.

The lavas of Los Gemelos and El Saladillo have microporphyritic hyalocrystalline vesicular texture and intersertal matrix. The phenocrysts and microphenocrysts are of olivine, clinopyroxene, plagioclase and micas. Spinels and apatite constitute accessory minerals, while calcite and iddingsite are the secondary phases. Remarkable features are the presence of quartz and feldspar xenocrysts and of xenoliths of metapelites and metasandstones in scoriae of the Gemelo Norte volcano. Vesicles (0.25 to 0.75 mm) are slightly elongated and irregular in shape.

Modal analysis carried out on thin sections of samples from the three volcanoes yielded the following average values: olivine (~ 9%), clinopyroxene (~ 9.7), spinels (~ 1.2%), micas (~ 0.8), and xenocrysts of quartz (~ 0.7%). Most of the grains, due to their small size have been computed as matrix (~ 78.6%), especially plagioclase, spinels and micas.

Olivine crystals (GN: $Fo_{87.2–74.4}$; ES: $Fo_{90.8–82.5}$; see Table 1) are euhedral to subhedral (0.1 to 4 mm), and commonly broken with fractures filled by calcite. Clinopyroxene coronas around olivine crystals (Fig. 4a) are common in response to reaction between the olivine and the liquid, note that an analysed clinopyroxene crystal gave ($En_{42.45}$ $Fs_{8.71}$ $Wo_{48.8}$) and is slightly depleted in silica compared to other isolated crystals. Spinels are the most frequent inclusions in olivine, apatite is less common. Some olivine crystals have iddingsite rims.

The plagioclase is an essential matrix component (GN: $An_{68–62}$; Fig. 5a; Table 1). Twinnings according to the albite and carlsbad laws are the most frequent. Scarce, anhedral to subhedral large (up to 1.8 mm) plagioclase crystals occur in samples from ES, some showing embayment, (Fig. 4b) others with corroded rims for what they are interpreted as xenocrysts. Some K-feldspars from El Saladillo were identified and yielded a $Or_{45–25}$ composition (Fig. 5a; Table 1); since this mineral phase is inconsistent with these type of rocks, they are also considered xenocrysts.

Clinopyroxene microphenocrysts (GN: $En_{46–48}$ $Fs_{7–10}$ $Wo_{44–45}$; ES: $En_{42–47}$ $Fs_{8–9}$ $Wo_{45–49}$: Fig. 5b; Table 2) are euhedral to subhedral with lengths ranging between 0.04 mm and 0.5 mm. They are usually twinned ({100} and hourglass twins) and frequently show glomerophyric texture. In addition, they appear as radial aggregates of microlites, in places where they reacted partially or completely with quartz xenocrysts. Phlogopite (0.1 to 0.4 mm) was detected by X-ray diffraction and by microprobe analyses; the individuals are subhedral and partially or totally replaced by opaque minerals. Spinels occur as opaque and translucent grains. Chemical analyses (Table 2) show that both chromite and magnetite are present. Chromite grains frequently form chain structures and are included in olivines, whereas magnetite is dispersed in the groundmass.

Table 1
Microprobe chemical analyses of olivines and feldspars

	OSI 22-El Saladillo											OSI 25-Los Gemelos (GN)						
Sample	Ol 1	Ol 2 c	Ol 2 r	Ol 3 c	Ol 3 r	Ol 4 c	Ol 4 r	Ol 5 c	Ol 5 r	Ol 6 c	Ol 6 r	Ol 1	Ol 2	Ol 3	Ol 4	Ol 5	Ol 6	Ol 7 c
SiO_2	52.024	41.275	40.891	40.03	40.303	39.921	38.458	41.65	40.468	40.408	40.398	40.045	40.017	37.201	39.567	40.041	40.311	39.092
TiO_2	0.718	0.021	0	0	0	0.002	0.054	0.018	0	0.011	0.022	0	0.004	0.033	0.034	0.042	0.013	0.053
Al_2O_3	1.935	0.024	0.036	0.033	0.046	0.022	0.004	0.025	0.016	0.025	0.009	0.013	0.008	0.018	0.038	0.025	0.014	0.026
Cr_2O_3	0.031	0.078	0.032	0.116	0.021	0.049	0.003	0.089	0.02	0.125	0	0.046	0.04	0	0.04	0.04	0.068	0.015
FeO	6.868	9.025	12.568	9.825	9.558	10.725	16.15	9.099	13.97	9.079	10.648	13.353	13.9	22.458	12.692	13.052	12.369	15.584
NiO	0	0.489	0.195	0.344	0.384	0.315	0.105	0.554	0.14	0.536	0.396	0.163	0.124	0	0.198	0.182	0.353	0.14
MnO	0.181	0.093	0.207	0.137	0.104	0.138	0.263	0.135	0.203	0.095	0.169	0.182	0.201	0.469	0.194	0.204	0.16	0.282
MgO	16.249	49.36	47.282	48.492	47.913	48.003	42.818	50.446	45.245	48.474	47.821	45.77	45.343	36.611	45.328	45.987	47.2	41.992
CaO	21.157	0.108	0.146	0.109	0.132	0.098	0.132	0.145	0.139	0.126	0.132	0.171	0.142	0.362	0.152	0.153	0.158	0.235
Na_2O	0.25	0.004	0.017	0.006	0.018	0.009	0	0.012	0	0.017	0.008	0.027	0.006	0.005	0	0.027	0.029	0.024
K_2O	0.016	0.007	0.004	0.006	0.004	0.003	0.002	0.001	0.01	0.006	0.021	0.02	0	0.008	0.009	0.017	0.01	0
BaO	0	0.062	0.075	0.212	0	0.025	0.074	0	0	0	0.04	0.147	0	0	0	0	0.027	0.199
SrO	0	0	0	0	0	0	0	0	0	0	0	0	0	0.043	0	0	0	0
Total	99.429	100.546	101.453	99.31	98.483	99.31	98.063	102.174	100.211	98.902	99.664	99.937	99.785	97.208	98.252	99.77	100.712	97.642
Si	1.288	1.004	1.001	0.992	1.003	0.992	0.994	0.998	1.008	1.001	1	1	1.002	1.001	1.002	1	0.995	1.011
Ti	0.013	0	0	0	0	0	0.001	0	0	0	0	0	0	0.001	0.001	0.001	0	0.001
Al	0.056	0.001	0.001	0.001	0.001	0.001	0	0.001	0	0.001	0	0	0	0.001	0.001	0.001	0	0.001
Cr	0.001	0.001	0.001	0.002	0	0.001	0	0.002	0	0.002	0	0.001	0.001	0	0.001	0.001	0.001	0
Fe	0.142	0.184	0.257	0.204	0.199	0.223	0.349	0.182	0.291	0.188	0.22	0.279	0.291	0.505	0.269	0.273	0.255	0.337
Ni	0	0.01	0.004	0.007	0.008	0.006	0.002	0.011	0.003	0.011	0.008	0.003	0.002	0	0.004	0.004	0.007	0.003
Mn	0.004	0.002	0.004	0.003	0.002	0.003	0.006	0.003	0.004	0.002	0.004	0.004	0.004	0.011	0.004	0.004	0.003	0.006
Mg	0.599	1.789	1.725	1.792	1.778	1.778	1.649	1.801	1.68	1.789	1.764	1.704	1.692	1.468	1.711	1.711	1.736	1.619
Ca	0.561	0.003	0.004	0.003	0.004	0.003	0.004	0.004	0.004	0.003	0.004	0.005	0.004	0.01	0.004	0.004	0.004	0.007
Na	0.012	0	0.001	0	0.001	0	0	0.001	0	0.001	0	0.001	0	0	0	0.001	0.001	0.001
K	0	0	0	0	0	0	0	0	0	0	0.001	0.001	0	0	0	0.001	0	0
Ba	0	0.001	0.001	0.002	0	0	0.001	0	0	0	0	0.001	0	0	0	0	0	0.002
Sr	0	0	0	0	0	0	0	0	0	0	0	0	0	0.001	0	0	0	0
MO	304.358	0.142	0.193	0.146	0.178	0.13	0.182	0.188	0.189	0.169	0.177	0.231	0.192	0.529	0.209	0.207	0.21	0.333
FO	325.179	90.736	87.001	89.793	89.995	88.848	82.447	90.855	85.21	90.553	88.893	85.965	85.305	74.385	86.422	86.253	87.218	82.78
FA	77.119	9.308	12.975	10.208	10.073	11.137	17.448	9.195	14.761	9.516	11.105	14.072	14.672	25.602	13.577	13.735	12.824	17.237
LI	0	0.485	0.194	0.343	0.39	0.315	0.109	0.539	0.142	0.54	0.397	0.165	0.126	0	0.204	0.184	0.352	0.149
TE	2.059	0.098	0.217	0.145	0.111	0.145	0.287	0.138	0.217	0.101	0.178	0.194	0.215	0.542	0.21	0.218	0.168	0.316
FM	0.196	0.094	0.132	0.103	0.102	0.113	0.177	0.093	0.15	0.096	0.113	0.142	0.149	0.26	0.138	0.139	0.13	0.175
Fo%	80.8	90.7	87.0	89.8	89.9	88.9	82.5	90.8	85.2	90.5	88.9	85.9	85.3	74.4	86.4	86.3	87.2	82.8
Fa%	19.2	9.3	13.0	10.2	10.1	11.1	17.5	9.2	14.8	9.5	11.1	14.1	14.7	25.6	13.6	13.7	12.8	17.2
#Mg	80.8	90.7	87	89.8	89.9	88.9	82.5	90.8	85.2	90.5	88.9	85.9	85.3	74.4	86.4	86.3	87.2	82.8

	OSI 25-Los Gemelos (GN)								OSI 22-El Saladillo	
	Pl 1 c	Pl 1 r	Pl 2 c	Pl 2 r	Pl 3 c	Pl 3 r	Pl 4 c	Pl 4 r	K-Feld 3	K-Feld 4
Na_2O	3.453	3.457	3.749	3.974	3.460	3.772	3.620	3.658	4.170	4.946
K_2O	0.346	0.345	0.458	0.498	0.376	0.492	0.363	0.385	7.285	4.047
SiO_2	51.180	51.162	52.063	52.188	51.440	52.265	50.841	51.120	63.314	60.326
Al_2O_3	30.725	30.994	29.922	29.945	30.810	30.135	30.809	30.615	19.865	23.082
BaO	0.100	0.014	0.000	0.185	0.199	0.043	0.099	0.028	0.411	0.439
SrO	0.260	0.096	0.266	0.327	0.246	0.218	0.300	0.245	0.000	0.007
CaO	13.705	13.877	12.802	12.805	14.020	13.208	13.899	13.428	3.178	5.895
FeO	0.606	0.697	0.876	0.757	0.742	0.817	0.762	0.747	1.078	1.298
Oxides total	100.375	100.642	100.136	100.679	101.293	100.950	100.693	100.226	99.301	100.040
Na	0.305	0.304	0.331	0.350	0.304	0.331	0.320	0.324	0.370	0.435
K	0.020	0.020	0.027	0.029	0.022	0.028	0.021	0.022	0.425	0.234
Si	2.331	2.323	2.373	2.371	2.328	2.366	2.316	2.333	2.896	2.736
Al	1.649	1.659	1.607	1.603	1.643	1.607	1.654	1.646	1.071	1.234
Ba	0.002	0.000	0.000	0.003	0.004	0.001	0.002	0.001	0.007	0.008
Sr	0.007	0.003	0.007	0.009	0.006	0.006	0.008	0.006	0.000	0.000
Ca	0.669	0.675	0.625	0.623	0.680	0.641	0.678	0.656	0.156	0.286
Fe	0.023	0.026	0.033	0.029	0.028	0.031	0.029	0.029	0.041	0.049
Cations	5.006	5.010	5.003	5.017	5.015	5.011	5.028	5.017	4.966	4.982
AB	30.682	30.450	33.702	34.931	30.207	33.106	31.371	32.282	38.903	45.518
OR	2.020	2.001	2.707	2.879	2.159	2.841	2.068	2.233	44.715	24.501
AN	67.298	67.549	63.591	62.191	67.633	64.053	66.561	65.485	16.382	29.980

c=core, r=rim, Ol=olivine, Pl=plagioclase, K-Feld=potassic feldspar.

Quartz xenocrysts (0.6 to 4 mm) are anhedral and generally fractured. The presence of clinopyroxene reaction coronas and/or corroded and embayed rims (Fig. 4c and d) is very common.

A remarkable feature is the occurrence of accessory lithics such as metasandstones and metapelites (Fig. 4e and f) from Puncoviscana Formation in proximal deposits (scoriae) of the Gemelo Norte volcano. Given the apparent absence of similar fragments in the lavas and the scarce reaction features between matrix and lithics margins, it is probable that they were incorporated in the magma during the explosive phase of the volcano (conduit opening).

The presence of chromite and apatite inclusions in olivine phenocrysts suggests that the former were the first

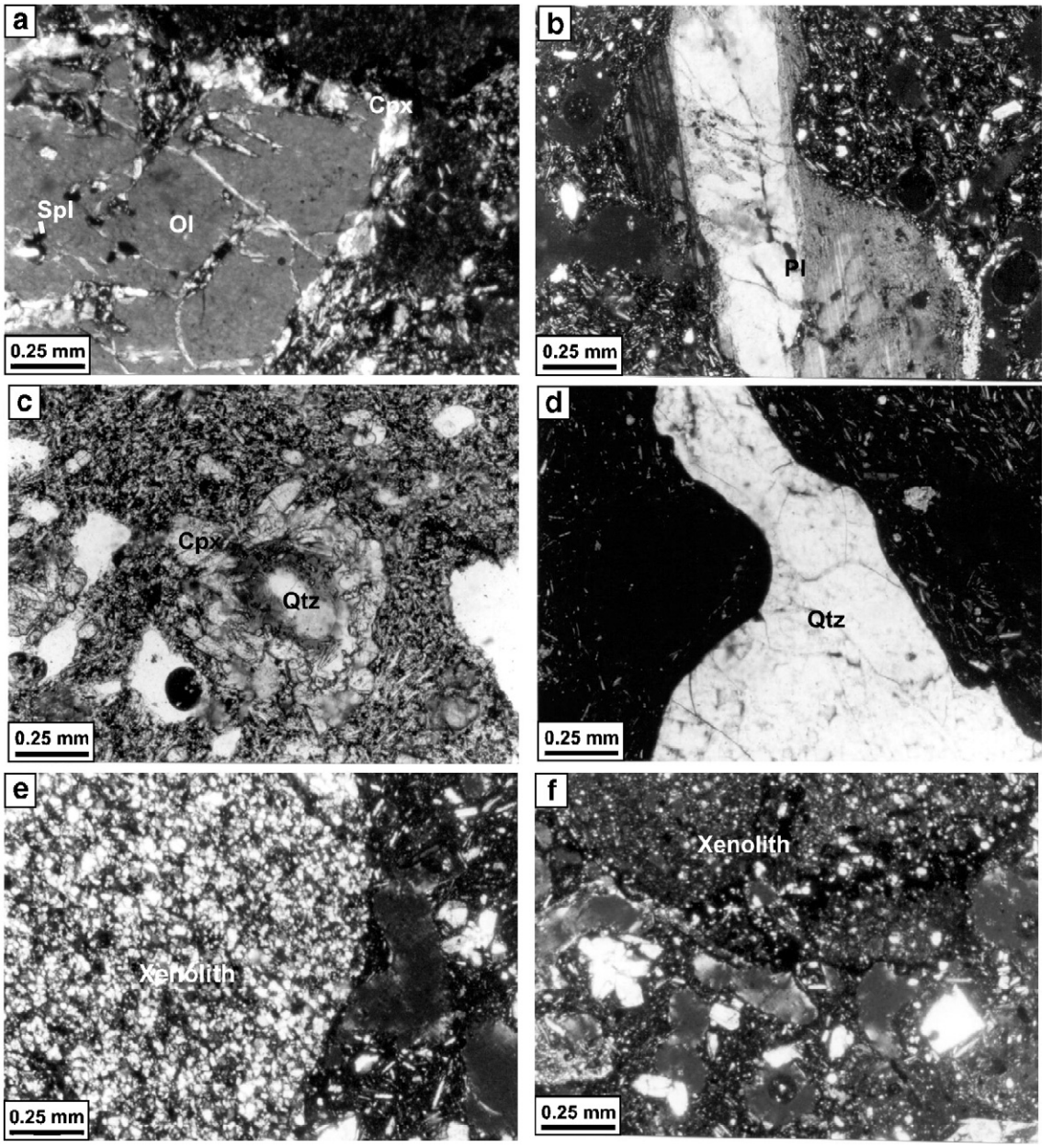

Fig. 4. Microphotographs of volcanic rocks. a) Olivine phenocryst with clinopyroxene reaction rim and spinels inclusions, sample OSI 24 (GS). b) Plagioclase xenocryst with embayment, sample OSI 21 (ES). c) Quartz xenocryst with clinopyroxene reaction corona, sample OSI 24 (GS). d) Embayed quartz xenocryst, sample from GN volcano. e) Metasandstone xenolith, sample form GN volcano. f) Metapelite xenolith, sample from GN volcano.

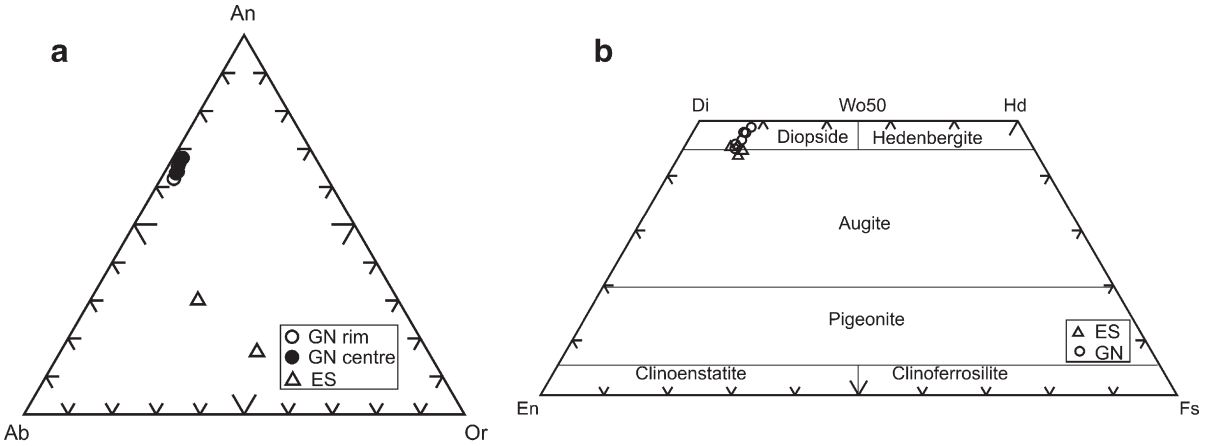

Fig. 5. Mineral classification diagrams. a) An–Or–Ab diagram. b) pyroxene classification diagram (En–Di–Hd–Fs) according to Morimoto (1988).

minerals to crystallize, followed by olivine. At more evolved stages, microphenocrysts and microlites of clinopyroxene and micas have formed, followed by plagioclase and some magnetite. Finally secondary minerals (iddingsite, calcite) have formed, surely in response to auto-alteration by a vapor phase and/or to weathering. Spinel-group minerals crystallized during the entire magma evolution history, but changed in composition from chromite in the early stages to magnetite in the more evolved ones.

In summary, petrographic evidence indicates that the magma interacted with felsic rocks. This is supported by: a) clinopyroxene reaction coronas in quartz xenocrysts, b) embayments in plagioclase, c) coronitic texture in olivines and d) embayments in quartz xenocrysts. The presence of xenoliths evidences the incorporation of these rocks towards the late-stage phases, probably during the conduit opening. However, the presence of partially dissolved xenocrysts of quartz and plagioclase requires that these minerals be incorporated at greater depths in order to allow more time for reaction. Moreover, we cannot reject the contamination with more lithics and xenocrysts at deeper levels, in which case they should probably reacted completely with the melt leaving no petrographical record but the variation in the whole-rock composition.

5. Geochemical characteristics

Samples were milled, powdered and dried at 105 °C for a period of 24 h. Loss on ignition (LOI) was determined at 950 °C until constant weight was achieved. Major elements were determined using fusioned tablets with $LiBo_4$ (1:6 concentration), while trace elements were determined on pressed powder tablets. Major elements and some trace elements were analysed by X-ray fluorescence with a wavelength-dispersive Rigaku 2000 system equipped with a Rh tube, detector SC and PC gas flow at the Universidad Nacional de Salta laboratory. Analyses of REE and some trace elements were performed by ICP-MS at the Instituto de Geociências, Universidade de Brasilia. The sample powder was fused with $LiBO_4$ (1/3) and the milled powdered glass dissolved in HNO_3 (3.5%). Concentrations were determined with a Finningan Element Magnetic Sector Mass Spectrometer, calibrated with international reference materials. Analytical quality was monitored with blanks and replicates of samples and standards. Analytical errors are below 5% of the concentration value. $^{87}Sr/^{86}Sr$ and $^{143}Nd/^{144}Nd$ isotopic ratios were measured at the Geochronology laboratory of the Instituto de Geociências, Universidade de Brasilia. Sm and Nd were processed and separated in ion exchange columns with LN-Spec resin and determined with a Finnigan MAT 262 spectrometer. The $^{143}Nd/^{144}Nd$ ratios were normalised to $^{146}Nd/^{144}Nd = 0.7219$ using the decay value of 6.54×10^{-12} a. The 2σ errors were 0.003% and 0.1%, for $^{143}Nd/^{144}Nd$ and $^{147}Sm/^{144}Sm$ respectively. Sr was first separated on a quartz column with Bio-Rad AG 50W-X8 200–400 resin and analysed in a Finnigan MAT 262 spectrometer. The 2σ error of $^{87}Sr/^{86}Sr$ was <0.017%.

Analytical results are shown in Table 3. In order to gain insight into the relationships with other related centres, we compared our data with those of Deruelle (1982, 1991), Knox et al. (1989), Kay et al. (1994), and Krallmann (1994). We selected San Jerónimo (SJ: 24° 14′S–66° 26′W) and Negro de Chorrillos (NCh: 24° 18′ S–66° 24′W) volcanoes because more analyses are available from these volcanoes than from other shoshonitic centres in the Argentine Puna. They are also monogenetic volcanoes, relatively close to ES and LGs,

Table 2
Microprobe chemical analyses of clinopyroxenes and spinels

	OSI 22-El Saladillo				OSI 25-Los Gemelos (GN)							OSI 22-El Saladillo					OSI 25-Los Gemelos (GN)				
	Cpx 1	Cpx 2 c	Cpx 3	Cpx 4	Cpx 1	Cpx 2	Cpx 3	Cpx 4	Cpx 5	Cpx 6*		Spl 1	Spl 2	Spl 3	Spl 4	Spl 5	Spl 1	Spl 2	Spl 3	Spl 4	Spl 5
SiO_2	51.96	53.224	51.871	51.799	50.233	49.079	51.007	48.404	50.931	47.563	SiO_2	0.175	0.08	0.185	0.524	2.392	0.038	1.379	0.073	0.081	0.226
TiO_2	0.621	0.772	0.7	0.505	1.097	0.829	0.778	1.303	1.257	1.716	TiO_2	11.585	10.855	12.223	2.248	6.91	1.752	16.141	2.183	9.775	14.293
Al_2O_3	1.898	2.553	2.649	2.13	4.166	2.833	2.732	5.122	4.695	5.763	Al_2O_3	3.377	3.305	2.777	9.489	3.733	17.628	2.88	15.789	4.567	2.781
Cr_2O_3	0.041	0.732	0.546	0	0.346	0.082	0.069	0.145	0.796	0.028	Cr_2O_3	7.494	10.86	5.299	41.084	19.563	33.27	0	32.844	15.269	0.018
Fe_2O_3	1.464	0	1.066	1.952	1.278	2.263	1.92	3.065	1.09	3.278	Fe_2O_3	34.182	32.858	33.383	11.666	29.539	11.904	29.781	13.472	28.507	35.794
FeO	5.512	5.088	4.35	5.658	4.897	4.354	4.675	4.441	4.907	4.731	FeO	34.783	34.658	35.056	21.212	31.18	24.385	39.407	25.462	32.841	37.24
NiO	0.013	0.013	0.073	0.029	0.005	0	0	0	0	0	NiO	0.102	0.098	0.012	0.101	0.063	0.092	0	0	0.057	0
MnO	0.197	0.1	0.075	0.215	0.08	0.15	0.204	0.133	0.137	0.183	MnO	0.487	0.576	0.486	0.508	0.52	0.677	0.366	0.684	0.72	0.464
MgO	16.304	16.246	16.17	15.737	15.006	15.116	15.871	14.216	14.798	13.452	MgO	3.849	3.661	3.319	7.67	3.304	6.5	2.625	5.882	4.079	3.404
CaO	20.963	22.121	21.383	21.208	21.548	20.743	21.128	21.513	22.506	21.532	CaO	0.328	0.099	0.372	0.079	0.222	0.096	1.578	0.073	0.098	0.165
Na_2O	0.209	0.298	0.404	0.274	0.371	0.292	0.28	0.34	0.37	0.391	ZnO	0	0.114	0.039	0.117	0.078	0.211	0.064	0.384	0.011	0.038
K_2O	0.023	0.009	0.023	0	0	0	0.037	0	0.017	0.041	V_2O_5	0	0.04	0.032	0.074	0.021	0.155	0	0.07	0	0.107
P_2O_5											Total	84.602	86.269	80.775	92	88.223	94.918	76.701	94.66	86.149	80.011
BaO	0.027	0	0	0	0	0.119	0.095	0	0.014	0											
SrO	0	0	0	0	0	0	0	0	0	0	Si	0.052	0.024	0.058	0.148	0.695	0.01	0.422	0.02	0.024	0.069
Total	99.232	101.156	99.31	99.507	99.027	95.86	98.796	98.682	101.518	98.678	Ti	2.608	2.428	2.861	0.478	1.51	0.357	3.711	0.451	2.187	3.298
											Al	1.192	1.159	1.019	3.165	1.278	5.634	1.038	5.106	1.602	1.006
Si	1.928	1.929	1.915	1.922	1.868	1.889	1.901	1.817	1.852	1.792	Cr	1.774	2.555	1.304	9.193	4.494	7.133	0	7.125	3.592	0.004
Ti	0.017	0.021	0.019	0.014	0.031	0.024	0.022	0.037	0.034	0.049	Fe^{3+}	7.701	7.356	7.82	2.484	6.458	2.429	6.852	2.782	6.383	8.265
Al	0.083	0.109	0.115	0.093	0.183	0.128	0.12	0.227	0.201	0.256	Fe^{2+}	8.709	8.623	9.126	5.02	7.576	5.53	10.076	5.843	8.173	9.557
Cr	0.001	0.021	0.016	0	0.01	0.003	0.002	0.004	0.023	0.001	Ni	0.025	0.023	0.003	0.023	0.015	0.02	0	0	0.014	0
Fe^{3+}	0.041	0	0.03	0.054	0.036	0.066	0.054	0.087	0.03	0.093	Mn	0.123	0.145	0.128	0.122	0.128	0.155	0.095	0.159	0.181	0.121
Fe^{2+}	0.171	0.154	0.134	0.176	0.152	0.14	0.146	0.139	0.149	0.149	Mg	1.718	1.623	1.54	3.236	1.431	2.627	1.196	2.406	1.809	1.557
Ni	0	0	0.002	0.001	0	0	0	0	0	0	Ca	0.105	0.032	0.124	0.024	0.069	0.028	0.517	0.021	0.031	0.054
Mn	0.006	0.003	0.002	0.007	0.003	0.005	0.006	0.004	0.004	0.006	Zn	0	0.025	0.009	0.024	0.017	0.042	0.015	0.078	0.002	0.009
Mg	0.902	0.878	0.89	0.87	0.832	0.867	0.882	0.795	0.802	0.755	V	0	0.008	0.007	0.014	0.004	0.028	0	0.013	0	0.022
Ca	0.833	0.859	0.846	0.843	0.859	0.855	0.844	0.865	0.877	0.869											
Na	0.015	0.021	0.029	0.02	0.027	0.022	0.02	0.025	0.026	0.029	#Mg	9.48	9.22	8.33	30.13	9.25	24.82	6.60	21.81	11.05	8.03
K	0.001	0	0.001	0	0	0	0.002	0	0.001	0.002											
Ba	0	0	0	0	0	0.002	0.001	0	0	0											
Sr	0	0	0	0	0	0	0	0	0	0											
WO	43.58	45.356	45.177	44.474	46.531	45.802	44.937	47.955	47.854	48.843											
EN	47.153	46.339	47.526	45.909	45.078	46.434	46.96	44.084	43.773	42.451											
FS	9.267	8.306	7.298	9.617	8.391	7.765	8.103	7.961	8.374	8.706											
FM	0.164	0.152	0.133	0.173	0.157	0.143	0.147	0.153	0.161	0.17											
#Mg	80.97	85.08	84.44	79.09	81.57	80.80	81.52	77.86	81.75	75.73											

*rimming OI 7 (see Table 1), c=centre, r=rim, Cpx=clinopyroxene, Spl=spinel.

and have been considered in conjunction with these as shoshonites by previous authors.

Rocks from Los Gemelos and El Saladillo volcanoes classify as trachybasaltic andesites, one sample from ES plotting in the trachyandesitic field of the TAS diagram (Le Maitre et al., 1989) (Fig. 6a). Analyses from both volcanoes plot within the shoshonitic series of Peccerillo and Taylor (1976) (Fig. 6b). It should be noted, however, that chemical classifications may not be entirely reliable in this case, since they may be influenced by the presence of quartz and feldspar xenocrysts. All the samples (Table 3) show high contents of Cr [495 to 265 ppm], Co [70 to 51 ppm], Ni [250 to 153 ppm] and MgO (9.93 to 7.32 wt. %), and high Mg number (Mg#) [65 to 72], indicating that they represent relatively primitive liquids. This is in good agreement with petrography and mineral chemistry; independently of their classification on the basis of major elements. Furthermore, most Harker diagrams depicted in Fig. 6c show poorly defined correlation of MgO with major and trace elements, suggesting that these magmas were not subject to extensive crystal fractionation.

The rare earth element contents were normalized to chondrite values (Fig. 7a) according to Sun and McDonough (1989). The shapes of REE patterns from different centres are similar, but samples from ES are slightly depleted in HREE compared to samples from LGs probably due to a slight difference in the source. Light (LREE) and medium (MREE) rare earth elements develop a steep slope, yielding $(La/Ho)_N$ values between 19.3 and 24 (Table 3); whereas the heavy rare earth elements (HREE) define a nearly null slope, with $(Er/Lu)_N$ between 1.1 and 1.18 (Table 3). The contrasting behaviour of Ce and Yb in Fig. 7b, where the negative correlation observed in samples from both Los Gemelos and El Saladillo volcanoes suggests that Yb has a compatible character suggests the retention of the HREE in residual garnet in the mantle source. On the other hand, the enrichment factor of ca. 10 times chondritic abundance for the heaviest REE suggests that the source area was previously enriched in incompatible elements.

The significant enrichment in LREE relative to chondrite, reaching La_N values between 266 and 382, corresponds to some of the highest values reported for the Central Andes (Schreiber and Schwab, 1991), this may be related with a major enrichment of the source in incompatible elements and very low degrees of partial melting. Moreover, in multi-element diagrams normalized to primitive mantle (not shown), a marked concentration of incompatible elements is also observed, especially of LILE (large ion lithophile elements).

The Eu anomaly is barely marked (Eu/Eu* ca. 0.9: Table 3), probably resulting from minor plagioclase and/or substantial clinopyroxene fractionation. Since plagioclase constitutes only microlites, it is interpreted as crystallizing towards the late stages of magma evolution, and therefore, could not be extensively removed from the magma to produce Eu anomalies.

Samples studied are characterized by high $^{87}Sr/^{86}Sr$ (0.70643 to 0.70772), $^{143}Nd/^{144}Nd$ ranging from 0.512365 to 0.512489, and negative εNd (−3 to −5) values. Pb isotopic ratios and Nd model ages (Table 3) indicate a significant participation of a crustal component and of an enriched mantle in the origin of these magmas.

In addition, the high $^{206}Pb/^{204}Pb$ isotopic ratios (Table 3) confirm assimilation of basement from the "south domain" (Wörner et al., 2002). Moreover, the lowest εNd values coincide with the highest T_{DM} values, being an additional evidence of basement participation in the formation of these magmas.

A comparative analysis between volcanoes of Calchaquí valley and those of SJ and NCh is difficult because (1) some of them (e.g. Negro de Chorrillos) have a wide range of values, overlapping the range of others; (2) there isn't a consistent tendency in the variations of isotopic ratios, major and trace elements, and overall petrographic characteristics between centres that are apparently very similar. This fact might be related to some slight differences in the source of these magmas and in the quantity/manner of crustal contamination.

Nevertheless, from comparative analysis, it comes out that SJ volcano has significant differences with the other volcanoes. First, when major elements are normalized almost all samples from SJ do not plot in the shoshonitic series of Peccerillo and Taylor (1976), but fall mostly inside the high-K calcalkaline series, classifying as high-K andesites, although they were previously regarded within the shoshonitic group (Knox et al., 1989; Kay et al., 1994). Second, the SJ mineral assemblage is also different from those of ES, LGs and NCh, since it contains hornblende and ortopyroxene. Third, SJ samples have lower Mg# (55 to 68) and chondrite normalized REE values.

Some magmas with the most primitive characteristics (high Mg#, high Cr and Ni contents) are the most contaminated with felsic basement in the $^{87}Sr/^{86}Sr$ vs. $^{143}Nd/^{144}Nd$ (Fig. 8a) and SiO_2 vs. $^{143}Nd/^{144}Nd$ (Fig. 8b) diagrams, whereas some with the most evolved characteristics are the least contaminated.

In this regard, we highlight for example, the behaviour of sample N16X (Deruelle, 1991) from NCh volcano, which shows the highest $^{143}Nd/^{144}Nd$ isotopic ratio and the lowest $^{87}Sr/^{86}Sr$ (Fig. 8a) ratio and silica content (Fig. 8b), for what it might be thought as the closest to a primitive magma composition within the considered set. Nevertheless, its

Table 3
Geochemical analyses

	El Saladillo			Los Gemelos						
				Third conduit	Gemelo Sur			Gemelo Norte		
Lat	24 33 33 S	24 33 58 S	24 33 57.9 S	24 45 33.6 S	24 45 22 S	24 47 23 S	24 45 24.5 S	24 44 49 S	24 44 05.2 S	24 44 36 S
Long	66 11 41W	66 11 37 W	66 11 37.9 W	66 09 54.2 W	66 10 25 W	66 10 36 W	66 10 23.0 W	66 10 37 W	66 09 58.5 W	66 10 3.5 W
Sample	OSI 21	OSI22	ES-001	LGs-001	OSI 24	OSI 26	LGs-003	OSI 25	LGs-005	LGs-004
SiO_2	54.54	55.35	54.53	51.87	53.35	53.26	51.75	52.60	51.92	51.23
Al_2O_3	14.39	13.64	13.66	14.41	13.90	13.95	14.08	14.16	13.81	14.08
Fe_2O_3	6.93	6.86	6.82	8.07	7.95	7.77	7.89	8.49	8.01	8.28
MnO	0.11	0.10	0.11	0.12	0.11	0.12	0.12	0.13	0.13	0.13
MgO	7.76	7.89	8.66	8.59	7.58	7.32	8.35	8.75	9.93	9.53
CaO	6.29	6.11	6.45	7.22	7.09	7.18	7.38	7.38	7.41	7.86
Na_2O	2.69	2.84	2.74	3.07	3.05	3.00	3.01	3.01	2.84	2.91
K_2O	3.98	4.20	4.19	3.45	3.96	3.99	4.01	2.89	3.34	2.90
P_2O_5	0.67	0.71	0.61	0.76	0.90	0.89	0.89	0.75	0.68	0.68
TiO_2	1.15	1.14	1.18	1.46	1.42	1.40	1.53	1.28	1.26	1.32
LOI	0.52	0.30	0.39		0.51	0.56	0.01	0.10		0.27
Total	99.01	99.14	99.35	99.03	99.82	99.44	99.00	99.56	99.32	99.18
Sc	23.16*	24.41*			23.92*	24.00*		25.02		
V	152.36*	149.71*	195	226	165.18*	167.26*	225*	182.26*	206	232
Cr	401.29*	406.91*	495	332	453.84*	265.46*	324	328.39*	404	398
Co	58.79*	50.80*	59	64	53.60*	50.80*	58	70.44*	60	58
Ni	219.06*	215.15*	246	195	167.85*	152.75	208	203.82*	250	237
Cu	119.89*	39.24*			38.44*	31.99*		37.23*		
Zn	64.70*	242.61*			105.36*	54.23*		78.71*		
Ga	19.92*	20.44*			20.37*	21.03*		20.69*		
Rb	121.82*	128.61*	93	75	126.12*	126.87*	83	85.32*	69	59
Sr	803.31*	846.18*	649	770	1,184.20*	1,194.96*	1,012	946.70*	755	743
Y	22.49*	22.51*	23	24	26.04*	26.51*	25	26.15*	24	23
Zr	315.68*	441.49*	292	279	409.91*	348.38*	330	276.83*	284	250
Nb	72.79*	60.82*	20	25	113.26*	38.99*	25	38.96*	23	24
Ba	1,465.87*	1,574.71*	1325	1005	1,605.70*	1,635.49*	1536	1,059.85*	1143	960
Hf	8.32*	12.16*			9.96*	8.92*		6.77*		
Ta	7.83*	1.76*			5.56*	3.38*		2.40*		
Th	11.72*	12.26*	8	9	18.59*	13.34*	10	12.21*	9	7
U	2.15*	2.45*			2.60*	2.55*		2.26*		1

La*	63.04	64.45			83.95	84.79		67.99		
Ce*	125.91	130.90			162.25	163.60		131.09		
Pr*	14.49	15.00			17.99	18.08		14.64		
Nd*	58.09	60.93			72.59	73.68		58.64		
Sm*	10.09	10.57			12.36	12.29		10.35		
Eu*	2.52	2.67			3.08	3.08		2.63		
Gd*	7.34	7.66			8.80	8.67		7.63		
Tb*	0.92	0.95			1.10	1.11		0.96		
Dy*	4.36	4.38			4.88	5.04		4.72		
Ho*	0.71	0.73			0.84	0.85		0.84		
Er*	1.87	1.88			2.08	2.15		2.13		
Tm*	0.28	0.28			0.30	0.31		0.32		
Yb*	1.78	1.74			1.91	1.91		2.03		
Lu*	0.25	0.25			0.29	0.28		0.29		
Sm (ppm)	9.867				11.734			9.581		
Nd (ppm)	55.2				67.23			54.14		
$^{147}Sm/^{144}Nd$	0.1080				0.1055			0.107		
$^{143}Nd/^{144}Nd$	0.512365+/−18				0.512424+/−14			0.512489+/−13		
εNd(0)	−5.32				−4.18			−2.9		
T_{DM} (Ma)	976				874			795		
$^{87}Sr/^{86}Sr$	0.70772+/−12				0.70697+/−5			0.70643+/−7		
$^{208}Pb/^{204}Pb$	38.45+/−0.28				39.12+/−0.24			39.0+/−0.6		
$^{207}Pb/^{204}Pb$	15.40+/−0.11				15.65+/−0.10			15.4+/−0.5		
$^{206}Pb/^{204}Pb$	18.42+/−0.14				18.72+/−0.12			18.6+/−0.4		
Eu/Eu*	0.89	0.91			0.90	0.91		0.90		
$(La/Ho)_N$	21.20	21.41			23.87	23.82		19.33		
$(Er/Lu)_N$	1.15	1.15			1.10	1.18		1.13		
$(La/Yb)_N$	25.40	26.98			31.53	31.84		24.02		
Mg#	68.95	69.52	71.58	67.85	65.40	65.13	67.73	67.14	71.08	69.53

*ICP-MS.

MgO, Ni, and Cr are beyond the lowest of the analysed set. Moreover, in Fig. 8c this sample is within the lowest Mg# values, for what it should be the most differentiated one.

On the other hand, sample OSI 21 from ES (and to a lesser extent sample 9.2.a from NCh) has the highest $^{87}Sr/^{86}Sr$ isotopic relations and the lowest $^{143}Nd/^{144}Nd$, i.e. the most crustal-contaminated signature, but its Cr, Ni and Mg# are among the highest. Furthermore, this sample has the most Cr-rich spinels and the most forsteritic olivines. It should be noted, however, that the tendency described for these samples does not verify for the entire compositional spectrum. Since the behaviour described above may also be

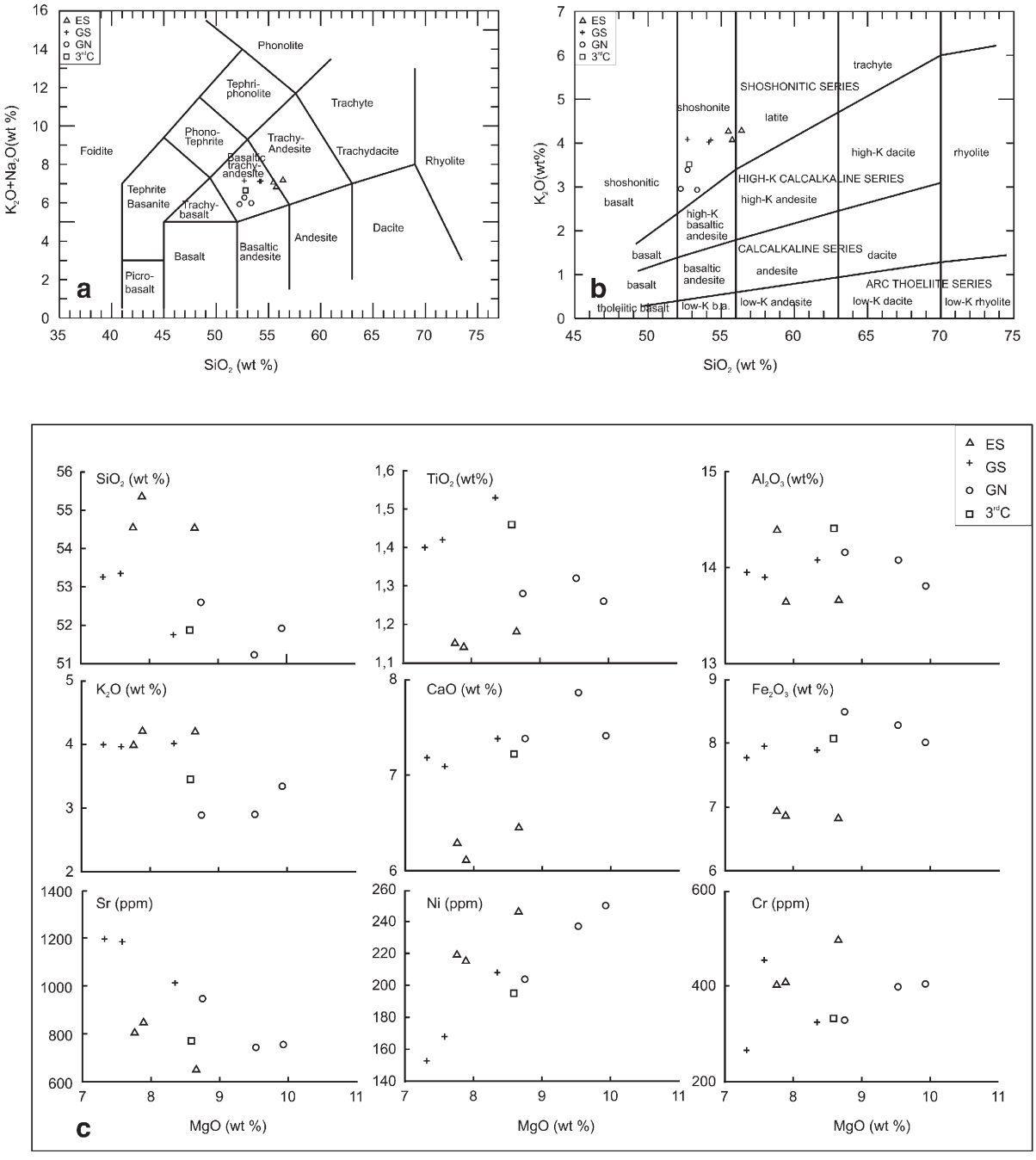

Fig. 6. Classification and Harker diagrams of whole-rock analyses. a) Total alkalis vs. silica (TAS) diagram, Le Maitre et al. (1989). b) Classification of Peccerillo and Taylor (1976). c) Variation of selected trace and major elements against MgO (wt.%) on Harker diagrams.

recognized within a single centre, it cannot be explained only by variation in the source, suggesting that contamination behaves randomly.

The sum of geochemical and physical properties indicate that the original magma came from the garnet stability zone and had crossed ca. 60 km of continental crust (Yuan et al., 2002) without any important fractionation (as demonstrated by their low crystal content, high Mg number, etc.)

This indicates a considerably high ascent velocity, without the establishment of shallow magma chambers, therefore precluding long crustal residence times. Notwithstanding, assimilation of essentially felsic crustal rocks is demonstrated by the presence and textural (dissolution) features of quartz and feldspar xenocrysts, as well as by geochemical features, and must have happened during ascent and within the conduits. This type of assimilation occurs if the magma has enough power to extract the country rock from the conduit, which, in turn, requires turbulent flow of the ascending magma and adequate geometric relations of the conduits (ATA: Moorbath and Thompson, 1980).

6. Age of Los Gemelos volcanoes and relations with tectonics

The Los Gemelos volcanoes were assigned to the Pleistocene–Early Holocene (Vilela, 1952) based on their field relations. To estimate the age of the LGs volcanoes we use stratigraphic relations and indirect absolute ages. Deposits of lacustrine origin overlie lavas from LGs. A lava flow from LGs volcanoes dammed the river valley and acted as a barrier leading to the formation of a small lake (Palmer, 1914; Trauth et al., 2000). The restricted dimension of this lake is indicated by the scarce outcrops of its deposits, which are set in a sub-horizontal paleotopography, and should not have suffered substantial erosion. The presence of lavas in

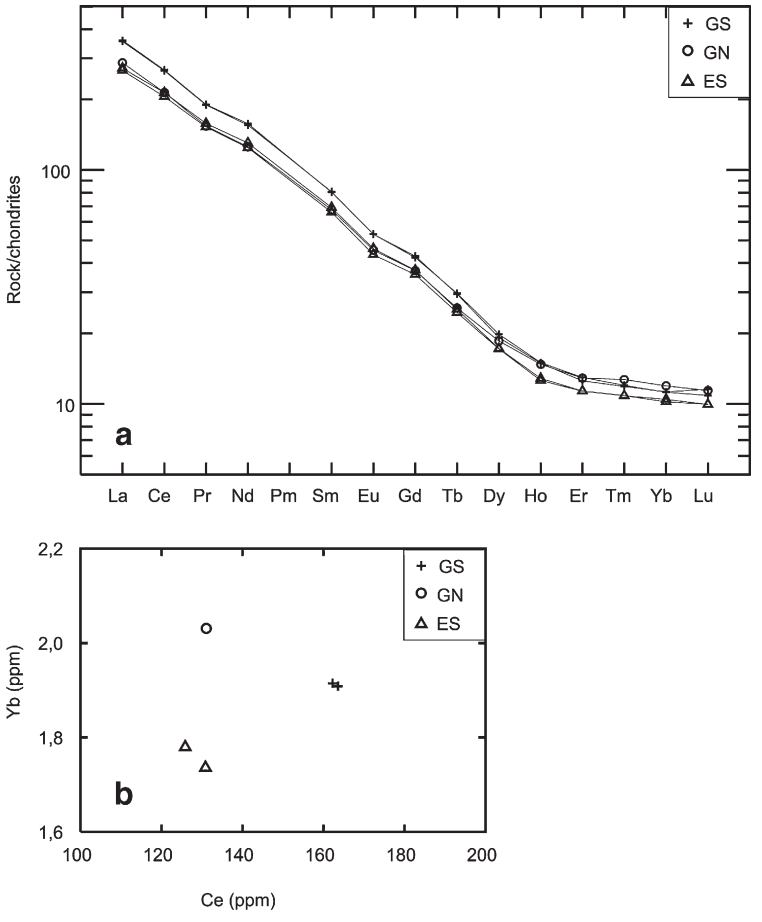

Fig. 7. a) REE diagram normalized to chondrite values of Sun and McDonough (1989). b) Ce vs. Yb diagram showing negative correlation between Ce and Yb for El Saladillo and Los Gemelos of La Poma.

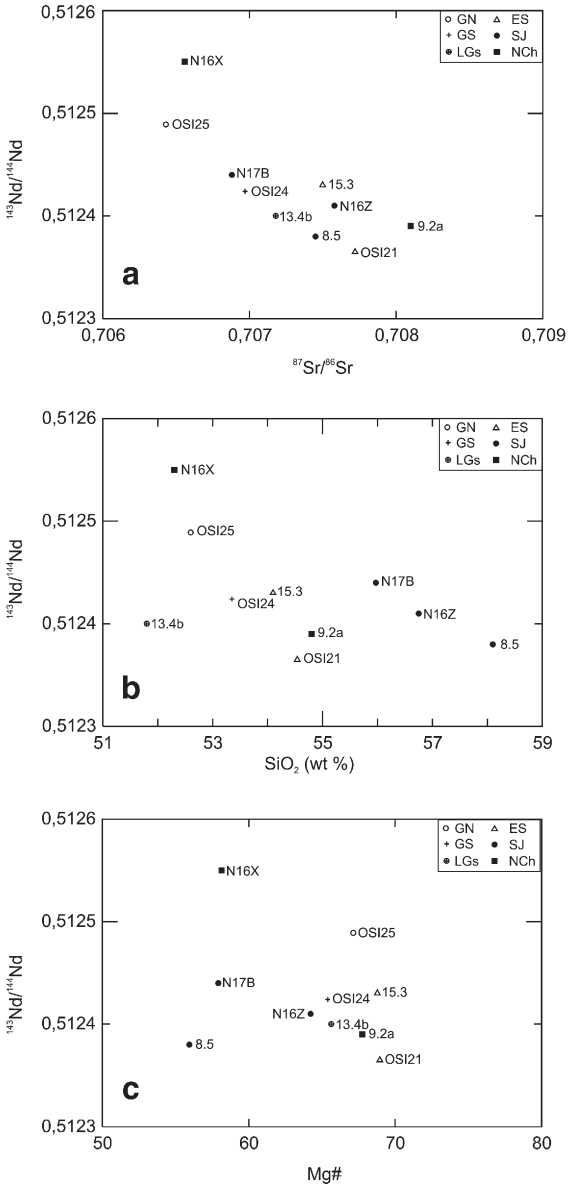

Fig. 8. a) Variation of $^{87}Sr/^{86}Sr$ vs. $^{143}Nd/^{144}Nd$. Note decreasing Nd relations with Sr relations increments. b) SiO_2 vs. $^{143}Nd/^{144}Nd$ diagram. c) #Mg vs. $^{143}Nd/^{144}Nd$. Samples: N16X, N17B, N16Z: Deruelle (1982, 1991); 15.3, 9.2a,13.4b, 8.5: Krallmann (1994).

both riversides evidences that the flow crossed the river. Moreover, lavas are found to the west of Calchaquí River, overlain by lacustrine deposits (Figs. 2a and 9). Trauth et al. (2000) dated organic matter from the basal layers of lacustrine sediments as 32,784±280 ^{14}C years BC, which provides a minimum age for volcanic activity at Los Gemelos. Moreover, the age of lacustrine sediments must be very close to the age of the lavas, given that the latter were responsible for the formation of the lacustrine deposit. Therefore, the volcanic event of LGs is about 35,000 years old.

It seems that there is an association between the magmatism and incremental tectonic activity. Regarding this, we have to consider that the age of Los Gemelos magmatism coincides with a peak in the occurrence of tectonic (Hermanns and Strecker, 1999; Marrett and Strecker, 2000) and/or climatic related paleolakes between 25,000 and 35,000 years (Trauth et al., 2000). To evaluate this relationship we discuss some morphometric parameters and flow directions, and their possible relation with the regional stress field (Nakamura, 1977; Tibaldi, 1995; Lagmay et al., 2000).

During the Pleistocene–Holocene, Los Gemelos zone was governed by a dextral strike-slip movement, as documented by some new measurements (Fig. 2a) and according to Marrett et al. (1994). Some relations between the general trend of the volcanic edifices and regional/local structures are highlighted below.

Cones are aligned ca. 10° from the Calchaquí Fault, coinciding with the strike in which a riedel *R* fault would form. Moreover, some of the cones flanks avalanches are among theoretical R and P faults as many other volcanoes (Lagmay et al., 2000). The elongation of cones and the breaching of the craters is perpendicular to the strike of the regional fault and is better explained as a response to the preexisting topographic slope (more than 10°) in which case the inference of tectonic causes can be masked (Tibaldi, 1995).

Other evidence of tectonic activity in the area are related with post-volcanic sedimentary deposits and their deformation. In this regard, we highlight that post-volcanic alluvial fans built up by successive debris flows are a common feature near Los Gemelos volcanoes. These flows start at the main fault plane and are perpendicular to its strike. They must have been originated in periods of increments in the tectonic activity of the region, which continues at present, as evidenced by the steepness of layers of modern alluvial fans and, more directly, by the magnitude 6 (INPRES: Instituto Nacional de Prevención Sísmica de Argentina) earthquake of 1930 that destroyed La Poma village. Elsewhere, Palmer (1914) reported previous seisms at La Poma.

In this tectonic context, the ascent of magma with the described characteristics requires a temporarily rigid behaviour of the lower crust to allow fracture propagation in sufficiently strong deformation regimes. At the same time, sufficiently deep, vertical and interconnected fractures must develop in the upper crust, to collect magma with the described characteristics and inhibit crystallization. Marrett and Emerman (1992) investigated the ascent of mafic Plio-Quaternary magma at the

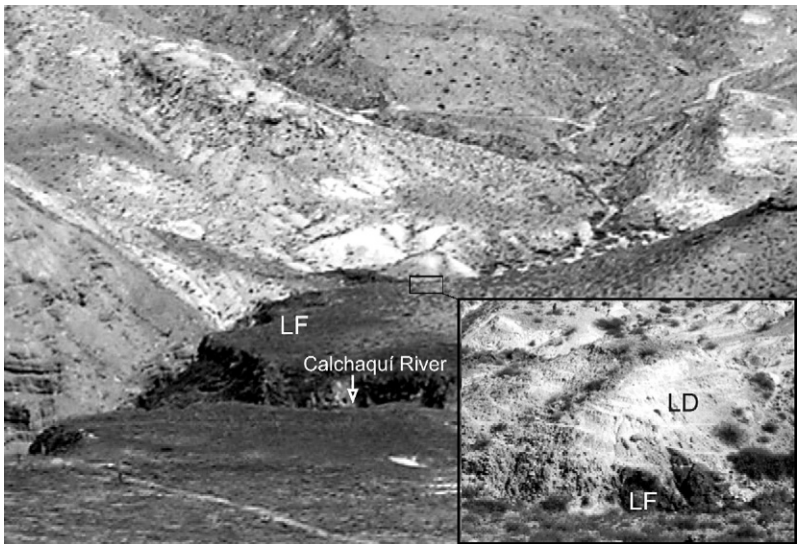

Fig. 9. The relationship between lava flows (LF) form Los Gemelos and the lacustrine deposits (LD) is highlighted.

southern Central Andes, proposing a combination of magmatic overpressure and a change in the regional stress field, from vertical extension to horizontal extension (strike-slip faults). Moreover, to achieve the ascent of magma from the base of the crust and its eruption at surface, like the studied case, high tectonic stresses are required (Watanabe et al., 1999), which characterize transpressive and transtensive environments (Saint Blanquat et al., 1998).

It is remarkable that the strike of some of the debris avalanches of volcanoes in the north of Chile (Francis and Wells, 1988) is coincident with the alignments of Los Gemelos (N 20°) and El Saladillo (N 160°). This might be an evidence that many of Andean volcanoes have emitted their products or collapsed in response to transpressive/transtensive local systems, analogous to the analysed case. However, an analysis of the Andean volcanoes as a whole must include a great variety of structural scenarios, hence their individual relation with respect to local structures remain largely unsolved.

In summary, considering: (1) the age of Los Gemelos volcanoes (~ 35,000 yr), (2) the temporal relation between Los Gemelos volcanoes and Calchaquí fault, (3) the relative synchronicity between the eruptions and the formation of a lake at La Poma, (4) the ages of other paleolakes of northwestern Argentina with a peak between 25,000 and 35,000 yr (Trauth et al., 2000), (5) debris flows as the causes of paleolake establishment (Trauth et al., 2000), (6) the favourable conditions for magma ascent in transpressive and transtensive systems (e.g. Saint Blanquat et al., 1998) and (7) the existence of paleolakes in proximal zones originated by increments in lateral ramps zones (Strecker and Marrett, 1999), it is possible to interpret a common tectonic cause for monogenetic eruptions, sector collapses and avalanches in northwestern Argentina.

7. Magma source and assimilation processes

Rocks from Los Gemelos volcanoes have been included in the so-called shoshonitic group by Knox et al. (1989) and later by Kay et al. (1994). The characteristics of this group are their high K_2O and incompatible elements contents and the development of very steep REE patterns. Knox et al. (1989) explain the genesis of these rocks by low percentages of partial melting of an enriched mantle above the subducted slab. More recently, Kay et al. (1994) consider an initial mafic magma mixed with crustal melts in a previously enriched, relatively thick, not delaminated lithosphere. On the other hand, Deruelle (1991) interprets the origin of magmas of San Jerónimo and Negro de Chorrillos volcanoes from partial melting of a peridotite, storage in deep crustal levels with possible assimilation of lower crust and, finally, contamination at upper crustal levels with incorporation of solid felsic materials.

Our data indicate relatively contrasting characteristics. On the one hand, there are features that are typical of a primary source (high Cr, Co, Ni and MgO content, high Mg #, presence of chromite and forsteritic olivine, and low viscosity). On the other hand, a marked crustal signature (high $^{87}Sr/^{86}Sr$ relations, negative εNd values, low $^{147}Sm/^{144}Nd$ relations) is evident. Some characteristics, such as the presence of phlogopite and the strong enrichment in LREE and, especially, in Sr, might be

indicative of an enriched mantle source. The high absolute content in incompatible elements, including REE is interpreted, in coincidence with Knox et al. (1989), as evidence of low rate of partial melting of a probably enriched source.

Contamination with crustal elements is often explained as the assimilation of fusible crustal constituents through AFC-type processes, for which it would be necessary that the magma was stored at some point within the crust for a substantial lapse of time. It is estimated that if a magma with the given physical and chemical characteristics as the ones studied here reached the surface, its time of crustal residence must have been very short, without the development of magma chambers. This, in turn, precludes extensive fractionation of crystalline phases and, consequently, renders AFC-type ineffective to explain the described features.

Moreover, we already stated that contamination in the studied volcanoes seems to behave randomly. This is clearly unexpected if the contamination with crustal material had occurred through an AFC-type process, where the more evolved magmas should be the most contaminated ones (Kerr et al., 1995).

Hence, and considering that (1) there is an evident contamination with crustal felsic material, (2) the contamination does not follow a progressive trend from primitive compositions towards evolved ones; instead, it behaves randomly, (3) although dissolved xenocrysts are common, whole xenoliths are scarce and were incorporated during the explosive phase, suggesting that assimilation was effective, and (4) the lowest calculated viscosities are in the most contaminated samples (in preparation), an ATA-type process (Assimilation during Turbulent Ascent, Moorbath and Thompson, 1980) is required to explain the observed contamination, independently of the relative enrichment of the original source.

8. Conclusions

The sum of the characteristics of the volcanic material is indicative of a strombolian eruption, with the construction of scoria and spatter cones at an initial explosive event, finishing with an effusive phase that breached the craters or emerged through conduits lateral to the cones.

Petrogenetically and on the base of available data it can be concluded that the volcanic rocks of Los Gemelos and El Saladillo were generated from a garnet-bearing mantle enriched in incompatible trace elements. The high concentration of incompatible elements, including the REE, denotes low percentages of melting. The presence of minerals such as chromite and forsteritic olivine, and the high content in Ni, Cr, Co and MgO indicate primary characteristics. Since 1) there is direct and indirect evidence for significant crustal assimilation, and 2) chemical and petrographic evidence (e.g. low crystal content, high magnesium number, absence of primary plagioclase phenocrysts) indicate that residence time (if any) was insufficient to allow extensive crystal fractionation and/or slow crustal wall rock assimilation by AFC, we interpret crustal contamination to have been produced during movement (ascent) of the magma mass in an approximately turbulent regime, through an ATA-type process.

Based on dating of lacustrine sediments overlying the lavas, the age of Los Gemelos volcanoes is assigned to the Upper Pleistocene, around 35,000 years.

Los Gemelos and El Saladillo volcanoes are associated with regional fractures that limit the Calchaquí valley. The original magmas ascended at great velocity due to magmatic overpressure, helped by high tectonic pressures typical of transpressive/transtensive environments. The ascent was through dykes related to fractures with strike-slip components, giving origin, on surface, to several aligned conduits. Cones alignment is parallel to R and R' directions in transpressive systems and coincides in part with some of the directions determined by Francis and Wells (1988) in volcanoes of the north of Chile.

Acknowledgments

This is a contribution to the IGCP 508 "Inception of volcano collapses by fault activity: examples from Argentina, Ecuador and Italy" and IGCP 455 "Effects of basement structural and stratigraphical heritages on volcano behaviour and implications for human activities". This project was funded by grants PICT98 N°03817, PEI N° 6089, PICT02 07-12417 and grants 1080/3, 1350/4 and 1288 from the CIUNSa. S. R. Guzmán thanks F. Hongn, R. Seggiaro and M. Arnosio for helpful discussions in the field. I. A. Petrinovic thanks the Secretaría de Minería y Recursos Energéticos de la Provincia de Salta (Argentina) for logistic support. J.A. Brod acknowledges a research grant from the CNPq-Brazilian Council for Research and Development, and additional funding by a CAPES-SECyT international cooperation project. Special thanks to R. Trumbull and an anonymous reviewer for their suggestions that improved the manuscript.

References

Barazangi, M., Isacks, B.L., 1976. Spatial distribution of earthquakes and subduction of the Nazca plate beneath South America. Geology 4, 686–692.

Deruelle, B., 1982. Petrology of the Plio-Quaternary volcanism of the south-central and Meridional Andes. J. Volcanol. Geotherm. Res. 14 (1–2), 77–124.

Deruelle, B., 1991. Petrology of Quaternary shoshonitic lavas of northwestern Argentina. In: Harmon, R.S., Rapela, C.W. (Eds.), Andean Magmatism and its Tectonic Setting. Geol. Soc. Am., Special Paper, vol. 265, pp. 201–217.

Francis, P.W., Wells, G.L., 1988. Landsat Thematic Mapper observations of debris avalanche deposits in the central Andes. Bull. Volcanol. 50, 258–278.

Hermanns, R.L., Strecker, M.R., 1999. Structural and lithological controls on large Quaternary rock avalanches (sturzstroms) in arid northwestern Argentina. Geol. Soc. Amer. Bull. 111 (6), 934–948.

Kay, S.M., Coira, B., Viramonte, J., 1994. Young mafic back arc volcanic rocks as indicators of continental lithospheric delamination beneath the Argentine Puna plateau, Central Andes. J. Geophys. Res. 99 (B12), 24323–24339.

Kerr, A.C., Kempton, P.D., Thompson, R.N., 1995. Crustal assimilation during turbulent magma ascent (ATA); new isotopic evidence from the Mull Tertiary lava succession, N.W. Scotland. Contrib. Mineral. Petrol. 119, 142–154.

Knox, W.J., Kay, S.M., Coira, B., 1989. Geochemical evidence on the origin of Quaternary basaltic andesites of the Puna, northwestern Argentina. Rev. Asoc. Geol. Argent. 34 (1–4), 196–206.

Krallmann, A., 1994. Petrographische und Geochemische untersuchungen an jungen, basischen vulkaniten im Bereich des Calama–Olacapato–El Toro lineamentes östlich der Vulkankette NW Argentinien. Ph thesis, Clausthaler Geowissenchaftliche Dissertationen H. 45, University of Clausthal, Germany.

Lagmay, A.M.F., Van Wyk de Vries, B., Kerle, N., Pyle, D.M., 2000. Volcano instability induced by strike-slip faulting. Bull. Volcanol. 62, 331–346.

Le Maitre, R.W., Bateman, P., Dudek, A., Kéller, J., Lameyre, J., Le Bas, M.J., Sabine, P.A., Schmid, R., Sorensen, H., Streckeisen, A., Woolley, A.R., Zanettin, B., 1989. A classification of Igneous Rocks and Glossary of Terms. Blackwell, Oxford.

Marrett, R.A., 1990. Late Cenozoic tectonic evolution of the Puna Plateau and adjacent foreland, northwestern Argentine Andes. Ph.D. Thesis, Cornell University, Ithaca.

Marrett, R.A., Emerman, S.H., 1992. The relations between faulting and mafic magmatism in the Altiplano–Puna plateau (central Andes). Earth Planet. Sci. Lett. 112, 53–59.

Marrett, R.A., Allmendiger, R.W., Alonso, R.N., Drake, R.E., 1994. Late Cenozoic tectonic evolution of the Puna Plateau and adjacent foreland, northwestern Argentine Andes. J. South Am. Earth Sci. 7 (2), 179–207.

Marrett, R., Strecker, M.R., 2000. Response of intracontinental deformation in the central Andes to Cenozoic plate reorganization. Tectonics 19, 452–467.

Mon, R., Salfity, J.A., 1995. Tectonic evolution of the Andes of northern Argentina. In: Tankard, A.J., Suarez Soruco, R., Welsink, H.J. (Eds.), Petroleum Basins of South America. Am. Assoc. Petr. Geol. Mem., vol. 62, pp. 269–283.

Moorbath, S., Thompson, R.N., 1980. Strontium isotope geochemistry and petrogenesis of the Early Tertiary lava pile of the Isle of Skye, Scotland and other basic rocks of the British Tertiary Province: an example of magma crust interaction. J. Petrol. 2, 217–231.

Morimoto, N., 1988. Nomenclature of pyroxenes. Subcommitee, IMA. Mineral. Mag. 52, 535–550.

Nakamura, K., 1977. Volcanoes as possible indicators of tectonic stress orientation—principle and proposal. J. Volcanol. Geotherm. Res. 2 (1), 1–16.

Palmer, H.S., 1914. Geological notes on the Andes of northwestern Argentina. Am. J. Sci. 38, 309–330.

Peccerillo, R., Taylor, S.R., 1976. Geochemistry of Eocene calc-alkaline volcanic rocks from the Kastamonu area, northern Turkey. Contrib. Mineral. Petrol. 58, 63–81.

Petrinovic, I.A., Riller, U., Brod, J.A., 2005. The Negra Muerta Volcanic Complex, southern Central Andes: geochemical characteristics and magmatic evolution of an episodic volcanic centre. J. Volcanol. Geotherm. Res. 140 (4), 295–320.

Riller, U., Oncken, O., 2003. Growth of the central Andean Plateau by tectonic segmentation is controlled by the gradient in crustal shortening. J. Geol. 111 (3), 367–384.

Riller, U., Greskowiak, J., Ramelow, J., Strecker, M., 1999. Dominant modes of Andean deformation in the Calchaquí river Valley. NW-Argentina. XIV Congreso Geológico Argentino, Salta. Actas, pp. 201–204.

Saint Blanquat, M., Tikoff, B., Teyssier, C., Vigeresse, L.J., 1998. Transpressional kinematics and magmatic arcs. In: Holdsworth, R.E., Strachan, R.A., Dewey, J.F. (Eds.), Continental Transpressional Tectonics Geological Society, London, Special Publications, vol. 135, pp. 327–340.

Schreiber, U., Schwab, K., 1991. Geochemistry of Quaternary shoshonitic lavas related to the Calama–Olacapato–El Toro Lineament, NW Argentina. J. South Am. Earth Sci. 4 (1/2), 73–85.

Strecker, M.R., Marrett, R., 1999. Kinematic evolution of fault ramps and role in development of landslides and lakes in intermontane valleys of northwestern Argentina. Geology 27, 307–310.

Sun, S.S., McDonough, W.F., 1989. Chemical and isotopic systematics of oceanic basalts: implications for mantle composition and processes. In: Saunders, A.D., Norry, M.J. (Eds.), Magmatism in Oceans Basins. Geol. Soc. London. Soc. Pub., vol. 42, pp. 313–345.

Tibaldi, A., 1995. Morphology of pyroclastic cones and tectonics. J. Geophys. Res. 100 (b12), 24521–24535.

Trauth, M.H., Alonso, R.A., Haselton, K.R., Hermanns, R.L., Strecker, M.R., 2000. Climate change and mass movements in the NW Argentine Andes. Earth Planet. Sci. Lett. 179, 243–256.

Vilela, C.R., 1952. Acerca de la presencia de sedimentos lacustres en el valle Calchaquí. Rev. Asoc. Geol. Argent. 7 (4), 219–227.

Viramonte, J.G., Galliski, M.A., Araña Saavedra, V., Aparicio, A., García Camacho, L., Martín Escorza, C., 1984. El finivolcanismo básico de la depresión de Arizaro, provincia de Salta. IX Congr. Geol. Argentino. 1, 234–251.

Watanabe, T., Kayaguchi, T., Seno, T., 1999. Tectonic controls on ascent and emplacement of magmas. J. Volcanol. Geotherm. Res. 91, 65–78.

Wörner, G., Beck, A., Euterhues, K., Heber, V., Lezaun, J., 2002. Basement petrology and arc magmatism near the Arica Bend (northern Chile). In: Miller, H., Hervé, F. (Eds.), Zeitschrift für Angewandte Geologie, SH1. Geoscientific cooperation with Latin America. Rio de Janeiro, Brasil, pp. 363–370.

Yuan, X., Sobolev, S.V., Kind, R., 2002. Moho topography in the central Andes and its geodynamic implications. Earth Planet. Sci. Lett. 199, 389–402.